Three-dimensional characterization of laboratory scour holes around bridge piers

Ana Margarida Bento[1,2,3], Teresa Viseu[1], João Pedro Pêgo[2,3] and Lúcia Couto[1]

[1]Water Resources and Hydraulic Structures Division, Hydraulics and Environment Department, National Laboratory of Civil Engineering
1700-066 Lisboa
PORTUGAL
[2]Hydraulics, Water Resources and Environmental Division, Civil Engineering Department, Faculty of Engineering of the University of Porto
4400-465 Porto
PORTUGAL
[3]Interdisciplinary Centre of Marine and Environmental Research of the University of Porto, Matosinhos, Portugal
E-mail: ana.bento@fe.up.pt

Abstract: *The presence of a bridge foundation leads to the formation of a scour hole, from which entrainment and transport of sediments are controlled by the turbulent structures therein developed. Hence, once formed, these scour holes interfere significantly with the scouring process in several ways, for instance, by modifying the incoming flow patterns. Therefore, a three-dimensional survey of the scour hole and the characterization of the deposition features is essential for prevention and safety control purposes. To tackle this, scouring experiments around two oblong bridge piers were performed in a tilting flume of the Portuguese National Laboratory of Civil Engineering (LNEC), under live bed flow conditions. A comprehensive characterization of laboratory scour holes was performed by using two advanced image-based measuring techniques, namely the close-range photogrammetry and the Kinect V2 sensor. The produced 3D bed morphology models provided detailed measurements, with significant accuracy, with quite similar results between the characterization approaches.*

Keywords: *bridge scour, scour hole, sediment transport, image-based techniques.*

1. INTRODUCTION

The collapse of bridges may occur due to several reasons, being local scouring around its foundation the most common. Local scour occurs due to the formation of vortices around piers and abutments, resulting in the change of a unidirectional approach flow into the three-dimensional flow field impacting an erodible channel, such as a riverbed. The local scouring process is intrinsically dependent on bridge geometry, river channel morphology, and hydrologic regime, which are entirely site specific. The impact of the flow on the dynamical behaviour of the riverbed and its repercussion on the structural stability of bridge foundations has been receiving greater recognition and attention from scientists and engineers nowadays (Chiew *et al.*, 2020).

The scour mechanism around a bridge foundation depends, among others, on the approach flow intensity, which can be classified as either clear water or live bed. Although there is a wide number of studies on clear water scour condition, most of the scour-induced bridge failures occur during floods, where a significant sediment flux is transported by the river flow and the flow intensity is high. In live bed condition, the scour hole equilibrium depth, when the scour depth fluctuates around a mean value, is reached faster than in clear water condition. Since the knowledge of scour hole dimensions is imperative in determining the extent of countermeasures needed to prevent/control scour at piers, the development of different approaches and techniques for accurate characterization of its geometry is essential. It is also worth highlighting that a detailed investigation on the scour hole morphology is also needed for the numerical modelling of scouring (Bento *et al.*, 2018).

Therefore, the aim of the present research was to develop image-based measurements and data processing techniques in a laboratory environment for the characterization of the scour hole and deposition zones geometry caused by the presence of bridge pier models in a movable bed, under live

bed conditions. Oblong bridge pier models, made of rectangular round-nose concrete columns, were considered since it is the typical shape in Portuguese bridges, from the 19th and 20th centuries.

2. LOCAL SCOURING EXPERIMENTS

2.1. Experimental apparatus

Two local scouring experiments, reproducing the flow at the vicinity of bridge pier models embedded in a uniform sediment bed, were performed in a 40.7 m long, 2.0 m wide and 1.0 m deep glass-sided rectangular tilting flume (Figure 1), located at the National Laboratory of Civil Engineering (LNEC), Lisboa (Portugal).

(a) View from upstream (b) View from inside

Figure 1 - Tilting flume at LNEC.

Two bridge pier models, properly characterized by a three-dimensional coordinate measuring machine, MMC 3D, were used with widths (*W*) of 0.11 m and 0.14 m (henceforth called *Pier 11* and *Pier 14*, respectively). Oblong bridge pier models were chosen as their geometries replicate the typical shape of bridge foundations, most common in Portugal in the 19th and 20th centuries. They were installed at the middle cross-section of an existing sand recess, 5.0 m long and 0.4 m deep, filled with a uniform quartz sand, characterized by a mean sediment diameter, D_{50}, of 0.86 mm, a specific gravity, *s*, of 2.65, and a geometrical standard deviation, σ, of 1.28. The corresponding dimensionless sediment diameter ($W = \left[(s-1)g/\upsilon^2\right]^{1/3} \cdot D_{50}$, being *g* the gravity acceleration and υ the kinematic viscosity coefficient) was 21.7.

The sand adopted, the position and the geometrical characteristics of the bridge pier were chosen to avoid the sand bed gradation effect, and the flume sidewall effects on the scouring process. The non-ripple-forming sediment criterion was respected and the effect of non-uniformity of sediment on the depth of the scour hole was avoided (Lee & Sturm 2009). Sediment coarseness ratios (W/D_{50}) of 127.9 and 162.8 were obtained for *Pier 11* and *Pier 14*, respectively, which effects were not negligible according to recent studies (Lee & Sturm 2009). The influence of flume sidewall on the scour hole development was avoided since the relation $W/B < 10\%$ was verified, being *W* the pier width and *B* the flume width (Chiew & Melville 1987). At the inlet of the tilting flume, a metallic grid assured the development of a uniform approach flow distribution. At the upstream end of the recess box, a fine gravel mattress, 0.3 m thick and 0.2 m long, allowed a smooth and progressive transition, avoiding scouring at the transition between the fixed and the movable bed.

2.2. Devices, measured variables and instrumentation

This experimental study comprised the monitoring of the hydraulic variables and the temporal evolution of the scour depth at piers' front during the scouring experiments with a 95% of confidence interval. The approach flow discharge, Q, was regulated by the rotational speed of the pumping system and monitored by an electromagnetic flowmeter, with a rate accuracy of ± 0.25%. A sluice gate placed at the downstream end of the flume enabled the flow depth adjustment inside the flume. Two resistive probes, suitably deployed to not interfere with the experiments' development, allowed the monitoring of the approach flow depth during the scouring experiments. The signals from the resistive probes and the electromagnetic flowmeter were acquired at a sampling frequency of 25 Hz.

The scour depth was registered with the aid of limnimeters at the upstream faces of the bridge pier models, with an accuracy of ± 0.05 mm. The flume was equipped with three moving carriages that moved along the longitudinal axis of the flume on two precisely levelled rails. These allowed the access to the experimental area for measuring purposes, particularly for flow and scouring parameters. A comprehensive measurement system was adopted for the three-dimensional characterization of the scour and deposition zones at the piers' vicinity. It consisted of capturing images, with a 12 MP spatial resolution camera (Action Cam NK 3056 Full HD) and on acquiring scans, at the beginning and at the end of the experiments using two advanced image-based techniques, namely the close-range photogrammetry and the Kinect V2 sensor.

2.3. Experimental procedure

After the installation of the oblong bridge pier model, the recess box was filled with the sand and flattened before the flume was slowly filled with water to allow air entrapped in the sand to escape. The flow was then drained and the sand arranged once again. The pier models were protected with metallic plaques to preclude undesirable scour at the beginning of the experiments. The tilting flume was filled again by increasing the rotational speed of the associated pump and by gradually adjusting the level of the downstream sluice gate until reaching the desired hydraulic variables. Once the prescribed flow conditions were reached, the metallic plaques covering the sand were carefully removed initiating, thus, the local scouring experiment. Before the beginning of experiments, a careful inspection of all instrumentation and measuring supports was undertaken. During experiments, the scour depth time evolution was measured at the piers' front in line with the development of the scouring phenomena (higher periodicity was adopted for the first instants as scour develops more rapidly). Further details can be found in Bento (2021). Scan images and photos of the bed morphology were captured at two moments of the scouring experiments: at the flat (initial) and the eroded (final) bed stages for characterizing the scouring effects and its respective ensemble. The three-dimensional characterization comprises the application of two image-based techniques, specifically the close-range photogrammetry and the Kinect V2 sensor. Both approaches require the previous emptying of the flume and control points, deployed in specific locations of well-known dimensions for reliable results.

2.4. Hydraulic conditions and time duration

The scouring experiments were conducted under live bed flow conditions, hereinafter designated as *Exp_Pier 11* and *Exp_Pier14* (Table 1). Preliminary tests have shown that the sand particles start moving for conditions close to critical velocity predicted by Neill's formula (1967), which was thus used to establish experiments' hydraulic conditions. Table 1 depicts the main hydraulic variables concerning the approach flow, namely discharge (Q), depth (h), velocity (V), Froude number (Fr), flow Reynolds number ($Re = Vh/\upsilon$), and, the parameter respecting the relation with the obstacle: the pier Reynolds number ($Re_D = VW/\upsilon$). The flow discharge and the water levels within the flume of the experiments were acquired continuously. For this reason, the main hydraulic variables were estimated with a 95% confidence interval, in which the estimated error corresponded to the sample error. Further details regarding the data filtering methods tested and applied to the flow discharge time evolution can be found in Bento (2021).

The water depth, h, within the tilting flume was assigned as the arithmetic average of the resistive probes data. Similar analysis was performed for the assessment of the corresponding experiments' flow

intensities. This uncertainty analysis has shown that the variability of the parameters of flow discharge, flow depth and flow intensity had no impact on the final results, as can be observed in Table 1. Both experiments were performed under subcritical flow conditions (Fr < 1.0), whilst the flow and pier Reynolds numbers (Re and Re_D in Table 1) ensured the fully turbulent approach flows.

Table 1 - Hydraulic conditions of experiments *Exp_Pier11* and *Exp_Pier14*.

Experiment (-)	*Pier width* (m)	Q (m^3/s)	h (m)	V (ms^{-1})	I_f (-)	Fr (-)	Re (-)	Re_D (-)
Exp_Pier11	0.11	0.1226 ± $6x10^{-7}$	0.1453 ± $1x10^{-6}$	0.4222 ± $3x10^{-6}$	1.335 ± $1x10^{-5}$	0.2964 ± $5x10^{-6}$	61069 ± 0.3	46254 ± 0.4
Exp_Pier14	0.14	0.1244 ± $1x10^{-6}$	0.1570 ± $2x10^{-6}$	0.3964 ± $6x10^{-6}$	1.2626 ± $2x10^{-5}$	0.2575 ± $6x10^{-6}$	61977 ± 0.6	55281 ± 0.8

The time required to reach 90% of the respective equilibrium scour depth (t_{90}), dependent of the reference time (*tr*, given in Sheppard *et al.* 2011), was used as a basis criterion for the time duration of the scouring experiments. The estimates of 2.9 days for *Exp_Pier11* and 4.1 days for *Exp_Pier14* were in line with Liang *et al.* 2019's findings. Despite the estimated values for t_{90}, the former, *Exp_Pier11,* lasted 3.1 days and the latter, *Exp_Pier14,* only 1.8 days of the scouring process (roughly 44.4% of the planned duration). Mechanical faults have been responsible for the experiment's interruption.

3. SCOUR HOLE AND DEPOSITION ZONE CHARACTERIZATION

3.1. Close-range photogrammetry

Photographs of the scour hole and the surrounding affected area were acquired at a height of 0.50 m from the initial (flat) bed level, as considered in Bento *et al.* (2018). Those photo captures were then processed in a Structured from Motion (SfM) software, particularly *Agisoft Metashape Profesional Edition*, version 64 bit 1.6.3 to reconstruct the beds morphology models. Digital Elevation Models (DEM) were then extracted and post-processed. For a successful completion of the DEMs, a minimum photo quality of 0.70 and an image overlap of about 60% should be guaranteed. These features play a relevant role in the success of the different processing phases in the generation of the 3D bed morphology models, bed contour surfaces and profiles.

3.2. Kinect V2 sensor

The Kinect V2 sensor is composed by a projector and two internal cameras: one *infrared camera* and a *RGB camera*. The *infrared projector* transmits a predefined pattern of light, which is deformed based on the distance of various points of the area of interest from the sensor (at a vertical distance of 0.5 m). This deformed pattern is then captured by the *infrared camera* and is correlated against a reference speckle pattern projected on the surface at known distance from the sensor to build a 3D map of the object. The resulting point clouds were then introduced in the 3D net processing *CloudCompare* software, version 64 bit 2.11, to build topographic 3D maps and corresponding, contour surfaces and bed profiles. The scans acquired from the Kinect V2 sensor were spatially referenced with a resulting Root Mean Square Error (RMSE) kept lower than 0.03 for obtaining a reliable model.

4. RESULTS

4.1. Scour depths at piers' front

Figure 2 illustrates the scour depth at 0.05 m from the upstream faces of the pier models, as well as with the corresponding logarithmic scales.

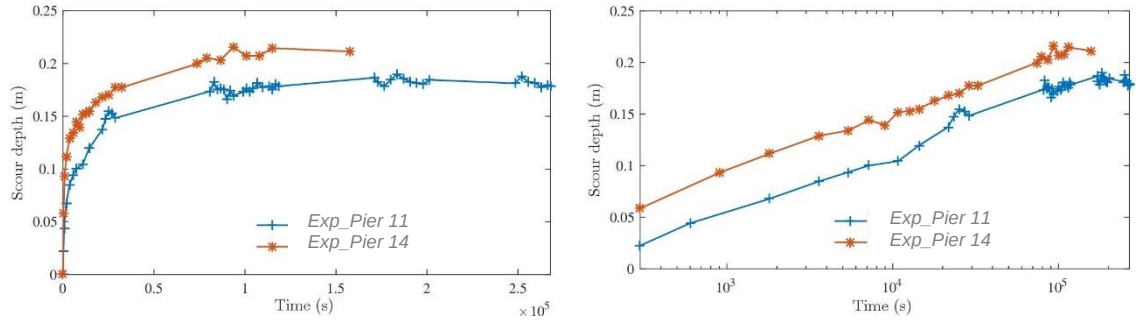

(a) Scour depth time evolution (b) Scour depth time evolution in logarithmic scale

Figure 2 - Temporal evolution of the scour depths at 0.05 m from the piers' front.

Evident differences were observed for the experiments (Figure 2). The higher width of *Pier 14* (*Exp_Pier14*) explained the temporal evolution of the scour depths towards higher scour depths than for *Exp_Pier11*. At the end of the first hour of *Exp_Pier11*, the measured scour depth attained was 0.085 m, whereas for *Exp_Pier14* such value almost reached the value of 0.13 m. The night period (of almost 11 hours, from the last measurement performed on the first day and the first one on the second day), registered an increase of the scour depth of 0.0225 m. During the second day experiments, a reduction of slope was visible. At the end of experiments, the final scour depths were 0.1790 m (*Exp_Pier11*) and 0.2114 m (*Exp_Pier14*). This latter scour depth, registered at roughly 1.8 days of *Exp_Pier14*, was higher than the correspondent scour depth of *Exp_Pier11*, as can be observed in Figures 2(a) and 2(b). These results were used for validation purposes of the image-based techniques.

4.2. Scour holes and deposition zones at piers' vicinity

Eight three-dimensional models of the bed morphology at the vicinity of the pier models were derived, either from the application of close-range photogrammetry or by using the KinectV2 sensor, at the beginning and at the end of experiments. Figure 3 depicts the eroded bed models around *Pier 11* and *Pier 14* for the two scouring experiments (*Exp_Pier11* and *Exp_Pier14*), highlighting the control points. The origin (*x,y,z*) = (0; 0; 0) was taken at the center of the pier at the flume mid-plane surface. The characterization of the flat condition of experiments allowed the assessment of the initial stage of the bed elevation model. Thus, on average, the elevations were 0.230 m for *Exp_Pier11* and 0.225 m for *Exp_Pier14* below zero. The bed morphology models (Figure 3) are quite similar despite slight differences due to the quality of captures and image-based techniques' accuracy, which was assessed based on the reference points of the respective models and their absolute coordinates. The application of the close-range photogrammetry technique returned position average errors of 0.79 mm and 0.63 mm (8.1% and 26.7% lower than D_{50}) for *Exp_Pier11* and *Exp_Pier14*, respectively.

The three-dimensional bed models allowed the creation of contour surfaces, displayed in Figure 4, as a function of scour depth-to-approach flow depth (*ds/h*). The contour surfaces obtained for *Exp_Pier11* (Figure 4(a) and 4(b)) present quite similar results, showing the maximum scour depth at the pier's front. However, by inspection of the 3D models (Figures 3(a) and 3(b)) it is possible to infer that the characterization given by the close-range photogrammetry technique was more reliable since a maximum scour depth of 0.20 m is closer to the measurement performed with the aid of a limnimeter at the end of the experiment. According to Figure 4(b), the maximum scour depth, given by the Kinect V2 sensor, resulted in 0.242 m, which corresponds to a difference of 26%. Such differences were responsible for the distinctive color shadows of Figures 4(a) and 4(b). The processing phases of the Kinect V2 sensor scans, for *Exp_Pier14,* did not allow a more accurate length characterization of the bed morphology, mainly at the upstream side of *Pier 14*, as it was performed by applying close-range photogrammetry. In this experiment, the close-range photogrammetric technique gave a little deeper scour depth immediately upstream the pier model; a difference of 0.009 m between approaches was achieved. Despite slight differences, the close-range photogrammetry technique remains the more reliable approach, as can be confirmed by the eroded bed models. There are some discontinuities, even though not significantly affecting the resulting 3D bed models. The non-feeding feature of the herein live bed scour experiments explains, in part, the bed elevations, at the upstream reach of the sand box, lower than the respective flat bed stages. In both experiments, the sand was transported beyond the working section and the concrete stretch floor, appearing accumulated on the downstream recess box.

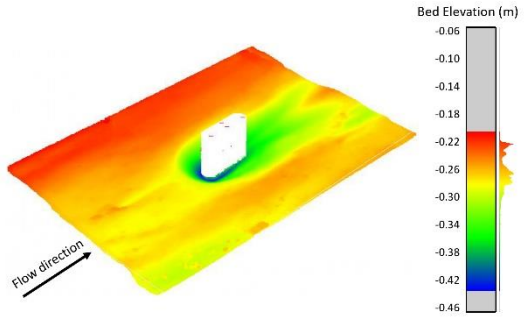

(a) *Exp_Pier11* – Photogrammetry

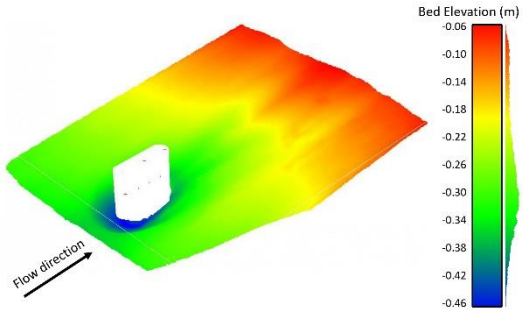

(b) *Exp_Pier11* – Kinect V2 sensor

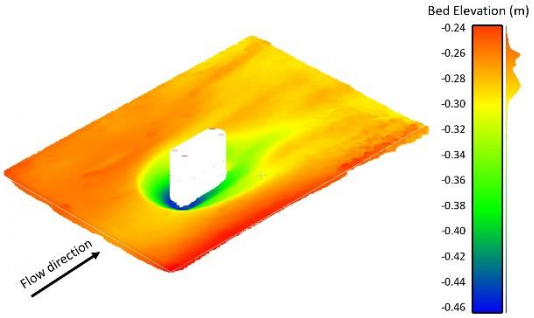

(c) *Exp_Pier14* – Photogrammetry

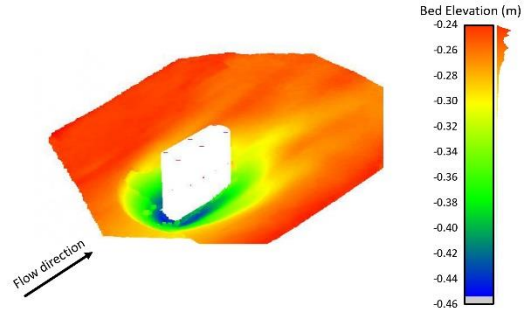

(d) *Exp_Pier14* – Kinect V2 sensor

Figure 3 - Three-dimensional eroded bed models from close-range photogrammetry (left panel) and Kinect V2 sensor (right panel).

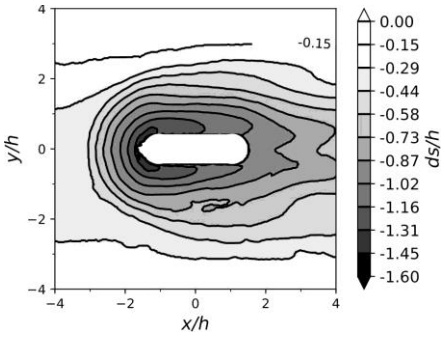

(a) *Exp_Pier11* – Photogrammetry

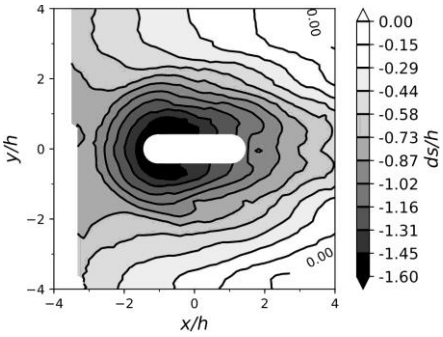

(b) *Exp_Pier11* – Kinect V2 sensor

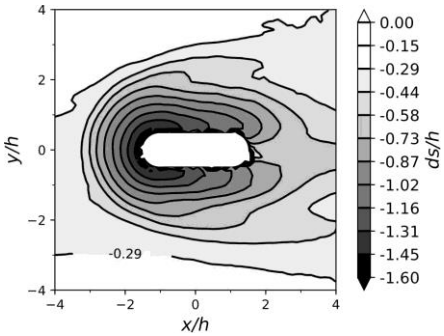

(c) *Exp_Pier14* – Photogrammetry

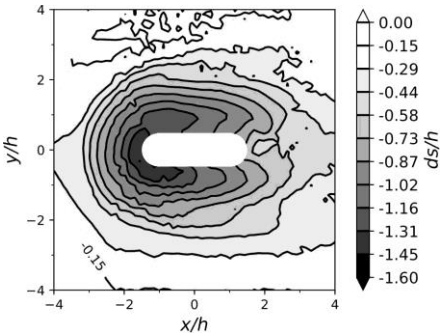

(d) *Exp_Pier14* – Kinect V2 sensor

Figure 4 – Contours of local scour around the bridge pier models from close-range photogrammetry (left panel) and Kinect V2 sensor (right panel).

4.3. Bed profiles

Figure 5 depicts the bed profiles considered in the present analysis. These profiles, at the vicinity of the pier models, are given in Figures 6 and 7. A direct comparison between the aforesaid techniques can thus be performed, as a function of the approach flow depth. Higher differences between the two image-based characterization techniques occurred for *Exp_Pier11* (Figure 6(a)); as aforementioned, the Kinect V2 sensor was returning erroneously higher scour depth values. For that experiment, the close-range photogrammetry technique revealed to be undoubtedly the more realistic as confirmed by the 3D model and the scour depth point-wise measurement performed at 0.05 m from the pier's front (Figure 6(a)).

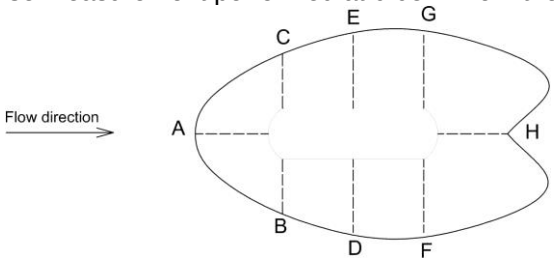

Figure 5 – Scheme of the scour bed profiles under analysis.

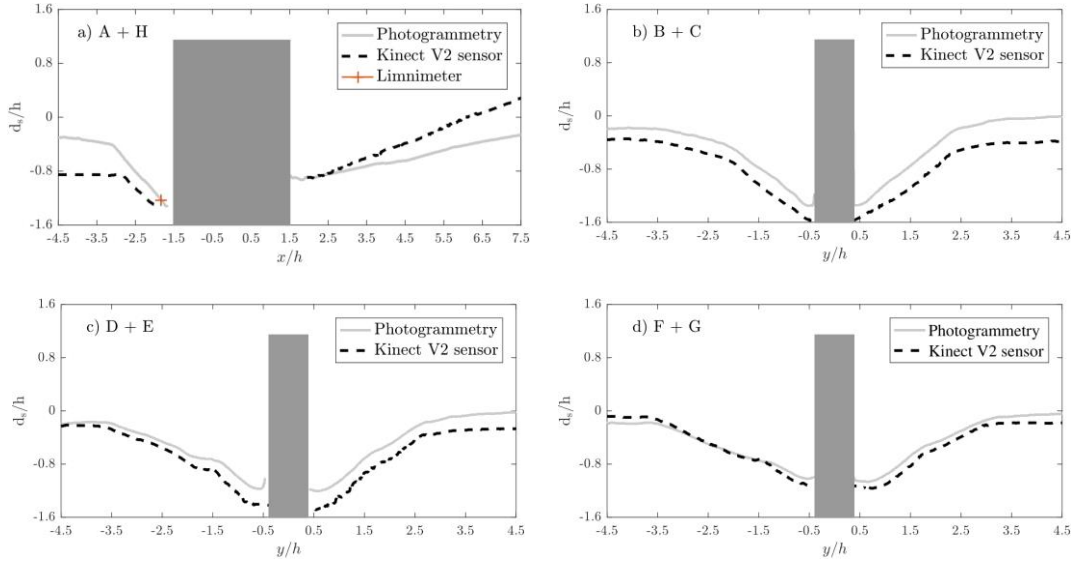

Figure 6 – Scour bed profiles from close-range photogrammetry (continuous line) and Kinect V2 sensor (dashed line) for *Exp_Pier11*.

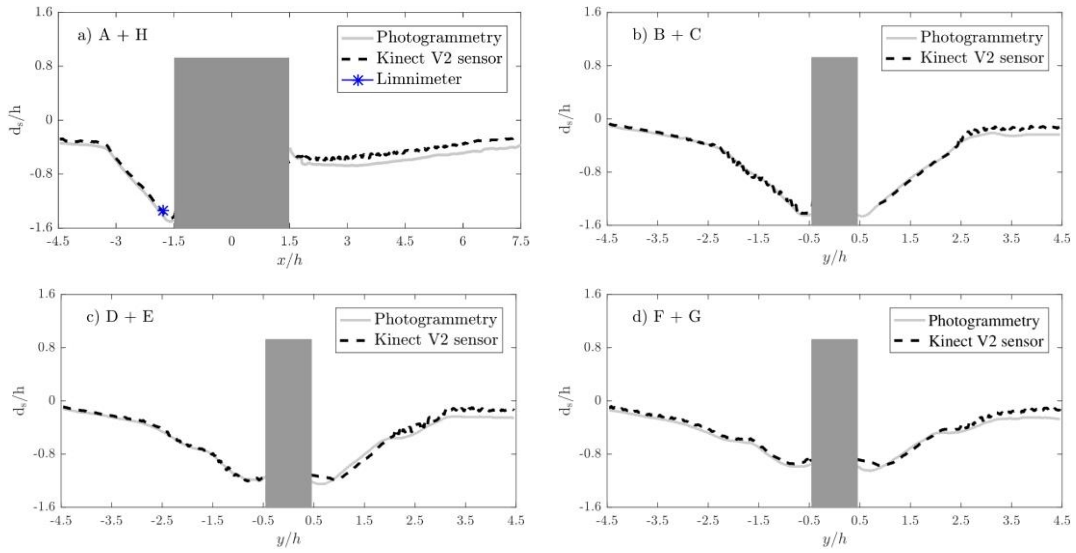

Figure 7 – Scour bed profiles from close-range photogrammetry (continuous line) and Kinect V2 sensor (dashed line) for *Exp_Pier14.*

5. CONCLUSIONS

The present paper presents scouring experiments around two oblong bridge piers, performed in a tilting flume of the Portuguese National Laboratory of Civil Engineering (LNEC), under live bed flow conditions, for the characterization of scour holes around the pier models, taking advantage of advanced survey and sensor technologies, by the three-dimensional (3D) point clouds and digital elevation models (DEMs). Eight three-dimensional maps of bed morphology at the vicinity of the pier models were derived at the beginning and the end of experiments. The produced 3D bed morphology models provided detailed measurements with quite similar results between the image-based techniques. In addition, bed contour levels and 2D bed profiles, both transversal and longitudinal, are given. Further, the obtained results indicate that the two image-based techniques, Kinect V2 sensor and close-range photogrammetry, can accurately monitor (once properly validated) the scouring process and replace the traditional point-wise measurement approaches for the full characterization of the scour hole and deposition zones around a bridge pier.

6. ACKNOWLEDGMENTS

The first author thanks the financial support of the Portuguese Foundation for Science and Technology through the PhD scholarship PD/BD/127798/2016, in the framework of InfraRisk Doctoral Program. This work was conducted in collaboration with the departments of Hydraulics and Environment and the Center of Scientific Instrumentation of the National Laboratory of Civil Engineering.This research was also supported by Centro Interdisciplinar de Investigação Marinha e Ambiental (CIIMAR) through the project with reference UID/Multi/04423/2019.

7. REFERENCES

Bento, A. M., Couto, L., Pêgo, J. P. and Viseu, T. (2018), *Advanced characterization techniques of the scour hole around a bridge pier model*, E3S Web of Conferences, vol. 40. EDP Sciences.

Bento, A. M. (2021), *Risk-based analysis of bridge scour prediction*, Ph.D. thesis, Faculty of Engineering of the University of Porto, Porto, Portugal.

Chiew, Y. M. and Melville, B. W. (1987), *Local scour around bridge piers,* Journal of Hydraulic Research 25(1), 15–26.

Chiew, Y.-M., Lai, J.-S., and Link, O. (2020), *Experimental, numerical and field approaches to scour research*, Water, 12(6), 1749.

Lee, S. O. and Sturm, T. W. (2009), *Effect of sediment size scaling on physical modelling of bridge pier scour*, Journal of Hydraulic Engineering 135(10), 793–802.

Liang, B., Du, S., Pan, X., and Zhang, L. (2019), *Local scour for vertical piles in steady currents: Review of mechanisms, influencing factors and empirical equations*, Journal of Marine Science and Engineering, 8(1), 4.

Neill, C. R. (1967), *Mean-velocity criterion for scour of coarse uniform bed-material*, 12th Proceedings Congress, vol. 3. Fort Collins, Colorado, USA.

Sheppard, D. M., Demir, H. & Melville, B. W. (2011), *Scour at Wide Piers and Long Skewed Piers*, vol. 682. Transportation Research Board.